Hybrid Method of Moments Solution for a Perturbed Dielectric Circular Cylinder

William D. Wood, Jr.
Department of Electrical and Computer Engineering
Air Force Institute of Technology
Wright-Patterson Air Force Base, Ohio, 45433

1 Abstract

A hybrid technique is developed, using the integral equation/moment method solution approach with non-free space Green's functions, for a class of scattering problems involving nearly-circular 2–D dielectric cylinders under TM_z illumination. The technique is applicable to other nearly-canonical 2–D penetrable scatterers, and may be extended to certain 3–D geometries. Applications to several 2–D geometries are demonstrated, with scattering predictions compared to those from a standard moment method code.

2 Introduction

The method of moments (MM) is one of the most powerful techniques for solving electromagnetic radiation and scattering problems in the frequency domain. Most implementations of the MM begin with invoking the surface or volume equivalence theorems, in which all material in the problem is replaced with free-space along with equivalent scattering currents. This results in an integral equation in which the unknown currents are integrated against the free-space Green's function.

The power of such a formulation lies in it's generality; the same free-space Green's function can be used for any geometry. However, in some cases, this generality comes at the expense of computational efficiency, since the unknown currents must span the volume or boundary of the scatterer. On the other hand, if the geometry under consideration is "close" to a canonical geometry for which the Green's function is known, then computational savings can be reaped if the integral equation is set up to exploit the Green's function. (For an excellent overview of this hybrid technique, see Newman [4].) An example of such a geometry is a nearly-circular, nearly-homogeneous ("perturbed") two-dimensional (2-D) dielectric cylinder.

In this paper, a hybrid Green's function/method of moments (GF/MM) solution will be presented for the plane-wave scattering from a perturbed dielectric cylinder in the TM_z polarization. First, the geometry of the perturbed dielectric circular cylinder will be defined. Second, the Green's function for the circular, homogeneous 2-D dielectric cylinder will be developed. Third, the integral equation for the scattering from the perturbed dielectric cylinder will be developed. Fourth, a volumetric pulse/point-matching MM solution will be presented. Fifth, numerical results will be presented for several representative perturbation geometries.

3 Geometry

Consider a dielectric circular cylinder with radius a and constant dielectric constant ε_c that is perturbed by an arbitrary protrusion and/or inclusion, as shown in Figure 1. We will denote the cross-section of the protrusion as Ω_p, and the cross-section of the inclusion as Ω_i. The protrusion material has relative permittivity ε_p, while the inclusion material has relative permittivity ε_i.

In the most general case, Ω_p represents any region outside the original circular cylinder, and Ω_i represents any region inside it. These perturbed regions can even be inhomogeneous (that is, ε_p and ε_i can vary within Ω_p and Ω_i, respectively), although ε_c must be a constant.

4 Green's Function

The Green's function for a circular, homogeneous dielectric cylinder is well known [7]. Ruck [6] uses it to give a formula, in terms of an infinite series, for the scattering width of a dielectric cylinder.

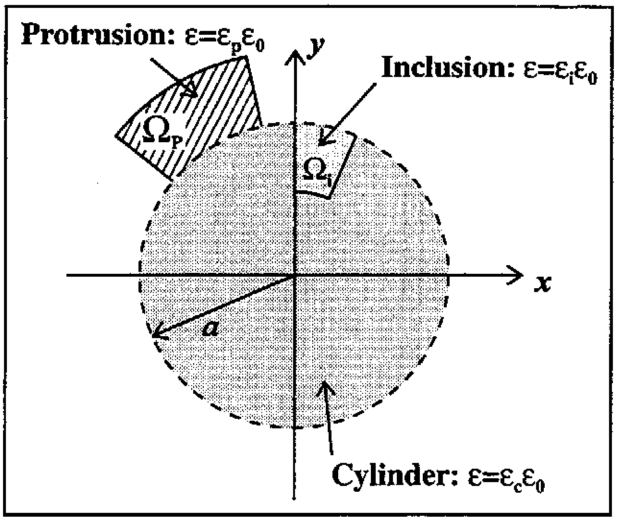

Figure 1: Perturbed Circular Cylinder Geometry

In general, for the TM_z polarization, the 2–D Green's function $G(\bar{\rho},\bar{\rho}')$ is proportional to the $\hat{z}$-directed electric field at observation point $\bar{\rho}$ due to a $\hat{z}$-directed monochromatic electric line source of unit strength at source point $\bar{\rho}'$. It obeys the inhomogeneous Helmholtz equation

$$\left(\nabla_t^2 + k^2\right) G(\bar{\rho},\bar{\rho}') = -\delta(\bar{\rho}-\bar{\rho}') \qquad (1)$$

where $\nabla_t^2 = \partial^2/\partial x^2 + \partial^2/\partial y^2$ and k is the propagation constant of the medium containing the observation point. The propagation constant outside the cylinder is $k_0 = \sqrt{\varepsilon_0\mu_0}$, while the propagation constant inside the cylinder is $k_1 = \sqrt{\varepsilon_c}k_0$, where ε_0 and μ_0 are the permittivity and permeability of free space, respectively. The time convention $e^{j\omega t}$ is assumed and suppressed. Finding the Green's function for an arbitrary geometry is generally non-trivial. However, if the geometry consists of a homogeneous, linear, isotropic dielectric circular cylinder centered at the origin and having radius a and relative dielectric constant ε_c, then the Green's function is reasonably straightforward to find by choosing it to obey the same boundary conditions as the electric field. Specifically, we choose $G(\bar{\rho},\bar{\rho}')$ to satisfy periodic boundary conditions in ϕ and continuity boundary conditions at $\rho = a$:

$$G(\bar{\rho},\bar{\rho}')|_{\phi=0} = G(\bar{\rho},\bar{\rho}')|_{\phi=2\pi} \qquad (2)$$

$$\left.\frac{\partial G(\bar{\rho},\bar{\rho}')}{\partial\phi}\right|_{\phi=0} = \left.\frac{\partial G(\bar{\rho},\bar{\rho}')}{\partial\phi}\right|_{\phi=2\pi} \qquad (3)$$

$$\lim_{\delta\to 0} G(\bar{\rho},\bar{\rho}')|_{\rho=a-\delta} = \lim_{\delta\to 0} G(\bar{\rho},\bar{\rho}')|_{\rho=a+\delta} \qquad (4)$$

$$\lim_{\delta\to 0} \left.\frac{\partial G(\bar{\rho},\bar{\rho}')}{\partial\rho}\right|_{\rho=a-\delta} = \lim_{\delta\to 0} \left.\frac{\partial G(\bar{\rho},\bar{\rho}')}{\partial\rho}\right|_{\rho=a+\delta} \qquad (5)$$

In addition, we expect the Green's function to obey the radiation condition as $\rho \to \infty$, and to remain bounded as $\rho \to 0$. The structure of the Green's function $G(\bar{\rho},\bar{\rho}')$ allows us to identify two components such that

$$G(\bar{\rho},\bar{\rho}') = G_0(\bar{\rho},\bar{\rho}') + G_s(\bar{\rho},\bar{\rho}') \qquad (6)$$

The first component, $G_0(\bar{\rho},\bar{\rho}')$, has the same form as the 2–D free-space Green's function and the second component, $G_s(\bar{\rho},\bar{\rho}')$, is an infinite series of eigenfunctions. The expression for $G(\bar{\rho},\bar{\rho}')$ takes on different forms depending on whether the source and observation points lie inside or outside the cylinder.

4.1 Case 1: $\rho, \rho' < a$

When both the source and observation points lie inside the dielectric circular cylinder (i.e., $\rho,\rho' < a$), the components of the Green's function are given by

$$G_0(\bar{\rho},\bar{\rho}') = -\frac{j}{4}H_0^{(2)}(k_1|\bar{\rho}-\bar{\rho}'|) \qquad (7)$$

$$G_s(\bar{\rho},\bar{\rho}') = \sum_{l=0}^{\infty} S_l^{(1)}(\rho,\rho')\cos[l(\phi-\phi')] \qquad (8)$$

where

$$S_l^{(1)}(\rho,\rho') = \frac{j}{4}\frac{\epsilon_l B_l}{A_l}J_l(k_1\rho)J_l(k_1\rho') \qquad (9)$$

$$A_l = J_l(k_1a)H_{l+1}^{(2)}(k_0a) - (k_1/k_0)J_{l+1}(k_1a)H_l^{(2)}(k_0a) \qquad (10)$$

$$B_l = H_l^{(2)}(k_1a)H_{l+1}^{(2)}(k_0a) - (k_1/k_0)H_{l+1}^{(2)}(k_1a)H_l^{(2)}(k_0a) \qquad (11)$$

$J_l(z)$ is the Bessel function of the first kind of order l and $H_l^{(2)}(z)$ is the Hankel function of the second kind of order l. The neumann number ϵ_l is defined as one when $l=0$ and zero when $l \neq 0$.

4.2 Case 2: $\rho, \rho' > a$

When both the source and observation points lie outside the dielectric circular cylinder (i.e., $\rho,\rho' > a$), the components of the Green's function are given by

$$G_0(\bar{\rho},\bar{\rho}') = -\frac{j}{4}H_0^{(2)}(k_0|\bar{\rho}-\bar{\rho}'|) \qquad (12)$$

$$G_s(\bar{\rho},\bar{\rho}') = \sum_{l=0}^{\infty} S_l^{(2)}(\rho,\rho')\cos[l(\phi-\phi')] \qquad (13)$$

where

$$\begin{aligned} S_l^{(2)}(\rho, \rho') &= \frac{j}{4}\frac{\epsilon_l C_l}{A_l} H_l^{(2)}(k_0\rho) H_l^{(2)}(k_0\rho') \quad (14)\\ C_l &= J_l(k_1 a) J_{l+1}(k_0 a) - \\ &\quad - (k_1/k_0) J_{l+1}(k_1 a) J_l(k_0 a) \quad (15) \end{aligned}$$

and the other quantities are as previously defined.

4.3 Case 3: $\rho < a < \rho'$ or $\rho' < a < \rho$

When the source and observation points lie in different regions (i.e., one inside and the other outside the dielectric cylinder), the components of the Green's function are given by

$$\begin{aligned} G_0(\bar{\rho}, \bar{\rho}') &= 0 \quad (16)\\ G_s(\bar{\rho}, \bar{\rho}') &= \sum_{l=0}^{\infty} S_l^{(3)}(\rho, \rho') \cos[l(\phi - \phi')] \quad (17) \end{aligned}$$

where

$$S_l^{(3)}(\rho, \rho') = \frac{1}{2\pi}\frac{\epsilon_l}{A_l} J_l(k_1\rho_<) H_l^{(2)}(k_0\rho_>) \quad (18)$$

$$\begin{aligned} \rho_< &= \min(\rho, \rho') \quad (19)\\ \rho_> &= \max(\rho, \rho') \quad (20) \end{aligned}$$

and the other quantities are as previously defined.

Equations 6, 7, 8, 12, 13, 16, and 17 specify the Green's function for an arbitrary pair of source and observation point locations in the presence of a homogeneous dielectric circular cylinder. The Green's function can now be used to formulate an integral equation for the case of the perturbed cylinder.

5 Integral Equation

Let us denote the total $\hat{z}$-directed electric field as the sum of generalized incident field E_z^{gi} and scattered field E_z^s components,

$$E_z(\bar{\rho}) = E_z^{gi}(\bar{\rho}) + E_z^s(\bar{\rho}) \quad (21)$$

where the generalized incident field is that field which would exist in the presence of the unperturbed cylinder. Invoking the volume equivalence principle [1], we may replace the perturbed geometry with the unperturbed cylinder along with an equivalent $\hat{z}$-directed electric current density $J_z(\bar{\rho})$. $J_z(\bar{\rho})$ is related to the total electric field by

$$J_z(\bar{\rho}) = j\omega\varepsilon_0 [\varepsilon(\bar{\rho}) - \tilde{\varepsilon}(\bar{\rho})] E_z(\bar{\rho}) \quad (22)$$

where $\varepsilon(\bar{\rho})$ is the relative permittivity of the perturbed geometry and $\tilde{\varepsilon}(\bar{\rho})$ is the relative permittivity of the unperturbed geometry. Note that J_z is nonzero only within the region $\Omega_p \cup \Omega_i$. The equivalent currents radiate the scattered field via the radiation integral

$$\begin{aligned} E_z^s(\bar{\rho}) &= L(J_z)\\ &= -j\omega\mu_0 \iint_{\Omega_p \cup \Omega_i} J_z(\bar{\rho}') G(\bar{\rho}, \bar{\rho}') d\bar{\rho}' \quad (23) \end{aligned}$$

where $G(\bar{\rho}, \bar{\rho}')$ is the Green's function of Equation (6).

Combining Equations (21), (22), and (23), we may write the integral equation

$$E_z^{gi}(\bar{\rho}) = \frac{J_z(\bar{\rho})}{j\omega\varepsilon_0 [\varepsilon(\bar{\rho}) - \tilde{\varepsilon}(\bar{\rho})]} - L(J_z) \quad (24)$$

6 Moment Method Solution

Let us approximate the unknown current density $J_z(\bar{\rho})$ using a pulse basis expansion,

$$J_z(\bar{\rho}) \approx \sum_{n=1}^{N} c_n P_n(\bar{\rho}) \quad (25)$$

where

$$P_n(\bar{\rho}) = \begin{cases} 1, & \bar{\rho} \in \Omega_n \\ 0, & \bar{\rho} \notin \Omega_n \end{cases} \quad (26)$$

and the non-overlapping set $\{\Omega_n\}_{n=1}^N$ spans $\Omega_p \cup \Omega_i$. We will further assume that $\varepsilon(\bar{\rho})$ is constant over each Ω_n. Since $J_z(\bar{\rho})$ is assumed constant over each Ω_n, these regions should be chosen to be reasonably small and squarish [5]. A good rule of thumb is that no linear dimension of Ω_n should exceed $\lambda/15$.

If we plug our expansion for $J_z(\bar{\rho})$ into the integral equation (24) and enforce it at the center of each pulse, we generate an N-by-N linear system of equations,

$$E_z^{gi}(\bar{\rho}_m) \approx \sum_{n=1}^{N} c_n \left[\frac{P_n(\bar{\rho}_m)}{j\omega\varepsilon_0 \Delta\varepsilon_m} - L_m(P_n)\right] \quad (27)$$

valid for $m = 1 \ldots N$ where

$$\begin{aligned} \Delta\varepsilon_m &= \varepsilon(\bar{\rho}_m) - \tilde{\varepsilon}(\bar{\rho}_m) \quad (28)\\ L_m(P_n) &= L(P_n)|_{\bar{\rho}=\bar{\rho}_m} \quad (29) \end{aligned}$$

Due to the sifting property of the pulse bases, the first term in brackets of Equation (27) is only active when $m = n$; that is, $P_n(\bar{\rho}_m) = \delta_{mn}$ where δ_{mn} is the Kronecker delta. Equation (27) can be expressed in matrix form as

$$\begin{bmatrix} E_z^{gi}(\bar{\rho}_1) \\ \vdots \\ E_z^{gi}(\bar{\rho}_N) \end{bmatrix} \approx \begin{bmatrix} Z_{11} & \cdots & Z_{1N} \\ \vdots & \ddots & \vdots \\ Z_{N1} & \cdots & Z_{NN} \end{bmatrix} \begin{bmatrix} c_1 \\ \vdots \\ c_N \end{bmatrix} \qquad (30)$$

where

$$Z_{mn} = \frac{\delta_{mn}}{j\omega\varepsilon_0\Delta\varepsilon_m} - L_m(P_n) \qquad (31)$$

for $m, n = 1 \ldots N$.

6.1 The Generalized Incident Field

Let the generalized incident field $E_z^{gi}(\bar{\rho})$ be caused by an electric line source of unit strength at $\bar{\rho}^i$. Thus,

$$E_z^{gi}(\bar{\rho}) = -jk_0\eta_0 G(\bar{\rho}, \bar{\rho}^i) \qquad (32)$$

where $\eta_0 = \sqrt{\mu_0/\varepsilon_0}$ is the impedance of free space. As $\rho^i \to \infty$, $E_z^{gi}(\bar{\rho})$ becomes indistinguishable from the excitation of a uniform plane-wave incident from the ϕ^i direction. Using the the large-argument asymptotic form of the Hankel function [3] in the Green's functions of sections 4.2 and 4.3, we find, for $\rho < a$,

$$\begin{aligned} E_z^{gi}(\bar{\rho}) \approx\ & \frac{\eta_0}{2\pi}\sqrt{\frac{2k_0}{j\pi\rho^i}}e^{-jk_0\rho^i} \times \\ & \sum_{l=0}^{\infty} \frac{\epsilon_l}{A_l} j^l J_l(k_1\rho)\cos\left[l(\phi - \phi^i)\right] \end{aligned} \qquad (33)$$

and for $\rho > a$,

$$\begin{aligned} E_z^{gi}(\bar{\rho}) \approx\ & \frac{-j\eta_0}{4}\sqrt{\frac{2k_0}{j\pi\rho^i}}e^{-jk_0\rho^i}\Bigg\{e^{jk_0\rho\cos(\phi-\phi^i)} - \\ & - \sum_{l=0}^{\infty} \frac{\epsilon_l C_l}{A_l} j^l H_l^{(2)}(k_0\rho)\cos\left[l(\phi - \phi^i)\right]\Bigg\} \end{aligned} \qquad (34)$$

6.2 The Scattered Field

Once the generalized incident field at the match points have been calculated and the elements of the $[Z]$ matrix have been found, then Equation (30) can be solved for the coefficients c_n. The scattered field at observation point $\bar{\rho}^o$ is then the sum of the fields radiated by the currents J_z and the field scattered by the unperturbed dielectric circular cylinder. Letting $\rho^o \to \infty$, we find

$$\begin{aligned} E_z^s(\bar{\rho}^o) \approx\ & -jk_0\eta_0\Bigg\{G_s(\bar{\rho}^o, \bar{\rho}^i) + \\ & + \sum_{n=1}^{N} c_n \int_{\Omega_n} G(\bar{\rho}^o, \bar{\rho}')d\bar{\rho}'\Bigg\} \end{aligned} \qquad (35)$$

Notice that we have purposely omitted the *direct* radiation from the source to the observation point. If we further assume that the far-field radiation of the scattering currents can be approximated by the far-field radiation of appropriately weighted line sources located at the match points, then we can write

$$\begin{aligned} E_z^s(\bar{\rho}^o) \approx\ & -jk_0\eta_0\Bigg\{G_s(\bar{\rho}^o, \bar{\rho}^i) + \\ & + \sum_{n=1}^{N} c_n(\text{Area}_n)G(\bar{\rho}^o, \bar{\rho}_n)\Bigg\} \end{aligned} \qquad (36)$$

where (Area_n) is the area of the n-th pulse basis function. The echo width of the perturbed cylinder is defined to be [2]

$$L_e = \lim_{\rho\to\infty} 2\pi\rho \left|\frac{E_z^s(\bar{\rho})}{E_z^i(\bar{0})}\right|^2 \qquad (37)$$

where $E_z^i(\bar{0})$ is the incident field at the origin produced by the line source at $\bar{\rho}^i$ radiating in free space. If we let the source and observer recede to infinity at the same rate ($\rho^i = \rho^o = \rho \to \infty$), then we can combine Equations (36) and (37) to write

$$\begin{aligned} L_e(\phi^i, \phi^o) \approx\ & \lim_{\rho\to\infty} 2\pi\rho \Bigg|\frac{G_s(\bar{\rho}, \bar{\rho})}{E_z^i(\bar{0})} + \\ & + \frac{\sum_{n=1}^{N} c_n(\text{Area}_n)G(\bar{\rho}, \bar{\rho}_n)}{E_z^i(\bar{0})}\Bigg|^2 \end{aligned} \qquad (38)$$

Equation (38) represents the bistatic echo width of a perturbed dielectric circular cylinder. If $\phi^i = \phi^o$, then Equation (38) gives the monostatic echo width.

7 Results

The hybrid GF/MM technique was tested against a standard surface integral equation MM (SIE MM) program for bistatic echo width predictions. The SIE MM program expands electric and magnetic surface currents along the perimeter of the homogeneous dielectric scatterer, using pulse basis functions and Galerkin testing. Each program was written in FORTRAN and executed on a Sun SPARCStation 2. Three perturbation geometries were chosen, each based on a dielectric circular cylinder having radius $a/\lambda_0 = 0.5$ and relative permittivity $\varepsilon_c = 2.0$. The bistatic echo width for the unperturbed geometry is shown in Figure 2, in units of dB relative to one free-space wavelength.

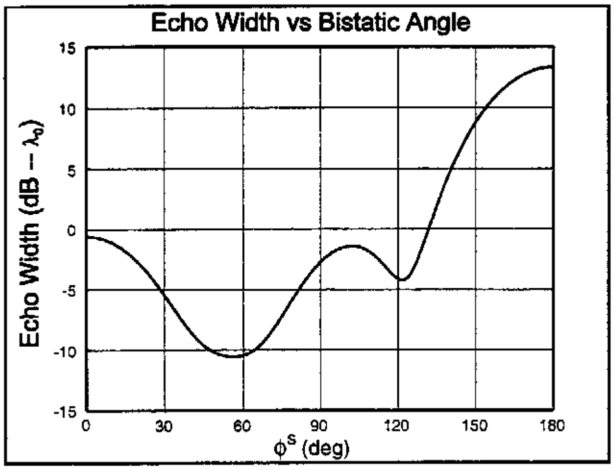

Figure 2: Bistatic Echo Width for Unperturbed Geometry: $a/\lambda_0 = 0.5$, $\varepsilon_c = 2.0$

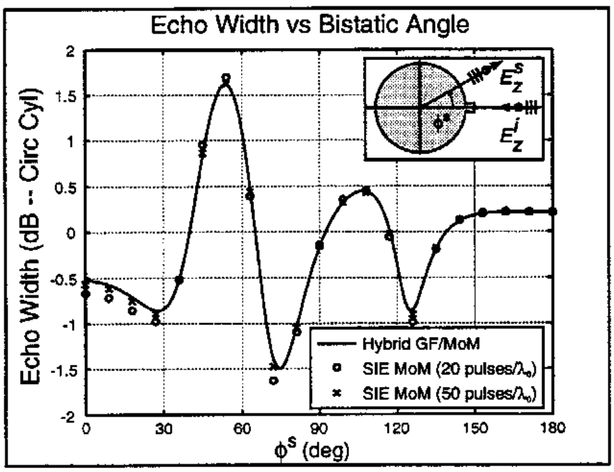

Figure 3: Bistatic Echo Width for Geometry #1: $a/\lambda_0 = 0.5$, $\varepsilon_c = 2.0$, $\Omega_p = \{\bar{\rho} : 0.5 < \rho/\lambda_0 < 0.6, -5° < \phi < 5°\}$.

The first perturbed geometry consists of a single protrusion on the right side of the dielectric circular cylinder, as shown in the inset of Figure 3. The protrusion extends from $\rho/\lambda_0 = 0.5$ to 0.6 , and from $\phi = -5°$ to $5°$. The protrusion material has relative permittivity $\varepsilon_p = 2.0$, so that the perturbed dielectric cylinder is homogeneous. Figure 3 shows the bistatic echo width for $\phi^i = 0°$ and ϕ^s from 0° to 180°. The bistatic echo width is plotted in units of dB relative to the bistatic echo width of the corresponding unperturbed dielectric circular cylinder (Figure 2). The results show that the SIE

Table 1: Computer Usage Summary

	Hybrid GF/MM		SIE MM		
Geometry	N	Time (sec)	Pulses per λ_0	N	Time (sec)
1	4	0.6	20	138	4.8
			50	340	47.9
2	8	1.9	20	148	5.5
			50	364	58.1
3	3	0.4	20	154	6.3
			50	376	63.7

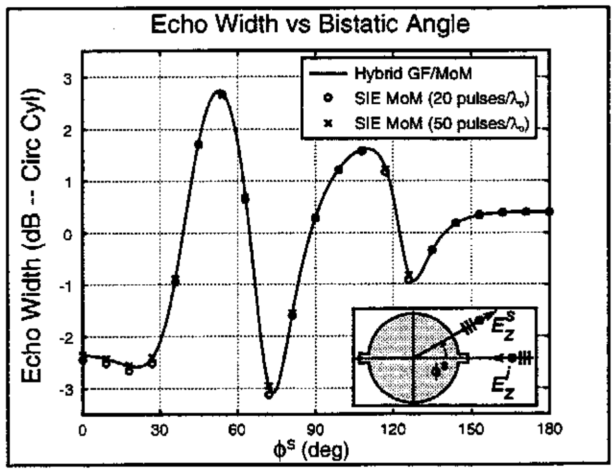

Figure 4: Bistatic Echo Width for Geometry #2: $a\lambda_0 = 0.5$, $\varepsilon_c = 2.0$, $\Omega_p = \{\bar{\rho} : 0.5 < \rho/\lambda_0 < 0.6, -5° < \phi < 5°, 175° < \phi < 185°\}$.

MM formulation requires 50 pulses per wavelength to achieve the accuracy of the hybrid GF/MM formulation with only 4 total unknowns. Table 1 shows that the hybrid GF/MM program executes nearly 80 times faster than the SIE MM program for this geometry.

The second perturbed geometry is similar to the first geometry, except that a second, identically-shaped protrusion is added to the left side of the circular cylinder. Figure 4 shows excellent agreement between the hybrid GF/MM and SIE MM formulations. As with the first geometry, the GF/MM program with 8 total unknowns gives nearly identical echo width predictions as the SIE MM program with over 300 unknowns. Table 1 shows that the hybrid GF/MM program executes nearly 30 times faster than the SIE MM program for this geometry.

The third perturbed geometry consists of a sin-

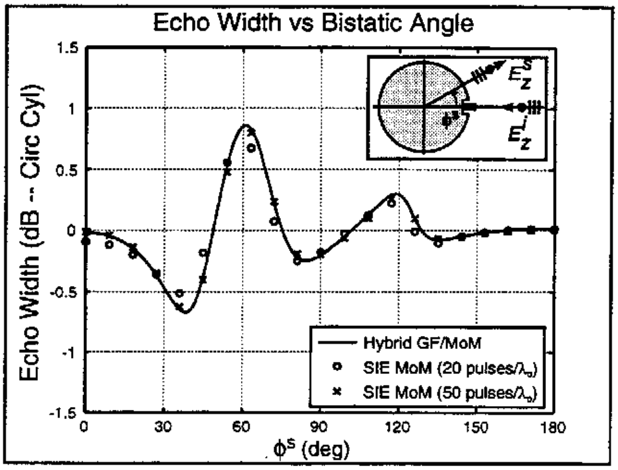

Figure 5: Bistatic Echo Width for Geometry #3: $a/\lambda_0 = 0.5$, $\varepsilon_c = 2.0$, $\Omega_p = \{\bar{\rho} : 0.5 < \rho/\lambda_0 < 0.567, -3.3° < \phi < 3.3°\}$, $\Omega_i = \{\bar{\rho} : 0.433 < \rho/\lambda_0 < 0.5, 3.3° < |\phi| < 10°\}$.

gle protrusion sandwiched between two identical inclusions. The protrusion occupies the region $0.5 < \rho/\lambda_0 < 0.567$ and $-3.3° < \phi < 3.3°$, and is filled with a dielectric having relative permittivity $\varepsilon_p = \varepsilon_c = 2.0$. The top and bottom inclusions occupy the regions $0.433 < \rho/\lambda_0 < 0.5$ and $3.3° < |\phi| < 10°$. Both inclusions are unfilled; that is, $\varepsilon_i = 1$. As shown in Figure 5, the hybrid GF/MM formulation with 3 unknowns gives nearly identical echo width predictions as the SIE MM formulation with over 350 unknowns. The time savings reaped by the hybrid GF/MM formulation relative to the SIE MM formulation exceeds 100.

8 Conclusions

This paper has presented a technique (the hybrid GF/MM) to increase the efficiency of the method of moments when calculating the scattering properties of geometries that are sufficiently "close" to a canonical geometry. The technique was developed in detail for the case of a homogeneous dielectric cylinder, although the technique may be applied to any penetrable geometry for which the Green's function can be found. Excellent agreement was shown between the hybrid GF/MM and standard MM formulations, and considerable savings in computer requirements were reported.

9 Acknowledgments

The author expresses his appreciation to Maj J. Paul Skinner for his expert guidance and insight in the development of the hybrid GF/MM technique.

References

[1] Balanis, Constantine A. *Advanced Engineering Electromagnetics.* John Wiley, New York, 1989.

[2] Harrington, Roger F. *Time-Harmonic Electromagnetic Fields.* McGraw-Hill, New York, 1961.

[3] M. Abramowitz and I. Stegun, editor. *Handbook of Mathematical Functions.* Number 55 in Applied Mathematics Series. U.S. Government Printing Office, Washington, D.C., 1972.

[4] Newman, E.H. An Overview of the Hybrid MM/Green's Function Method in Electromagnetics. *Proceedings of the IEEE,* 76(3):270–282, March 1988.

[5] Richmond, Jack H. Wave Scattering by a Dielectric Cylinder of Arbitrary Cross-Section Shape. *IEEE Transactions on Antennas and Propagation,* AP-13:334–342, May 1965.

[6] Ruck, G.T. *et al. Radar Cross Section Handbook,* volume 2. Plenum, 1970.

[7] Stratton, Julius A. *Electromagnetic Theory.* McGraw-Hill, New York, 1941.